USCAP

www.nature.com/labinvest

ARTICLE

CircRNA-ST6GALNAC6 increases the sensitivity of bladder cancer cells to erastin-induced ferroptosis by regulating the HSPB1/P38 axis

Li Wang[1,2], Shuiqing Wu[3], Haiqing He[3], Kai Ai[3], Ran Xu[3], Lei Zhang[3] and Xuan Zhu[3]✉

Previous studies have demonstrated that circST6GALNAC6 is a tumor suppressor in bladder cancer. However, the role of circST6GALNAC6 in ferroptosis remains unclear. In the current study, ferroptosis was induced in bladder cancer cells by erastin. Functional experiments showed that overexpression of circST6GALNAC6 promoted ferroptosis of bladder cancer cells in vitro and in vivo. Mechanistic studies revealed that circST6GALNAC6 bound to the N-terminus of small heat shock protein 1 (HSPB1) and thus blocked the erastin-induced phosphorylation of HSPB1 at the Ser-15 site, a phosphorylation site in the protective response to ferroptosis stress. In addition, protein kinase C inhibited circST6GALNAC6-induced ferroptosis by increasing the overall phosphorylation level of HSPB1, further demonstrating the role of phosphorylation activation of HSPB1 in resistance to ferroptosis. Finally, the involvement of the HSPB1/p38 MAPK pathway in the downstream signal transduction of circST6GALNAC6 in bladder cancer ferroptosis regulation was determined. The regulatory mechanism of ferroptosis sensitivity dependent on circST6GALNAC6 expression levels in bladder cancer was revealed as circRNA regulation of various protein functions. CircST6GALNAC6 inhibits HSPB1 and promotes cell ferroptosis by occupying the phosphorylation site (Ser-15) of HSBP1 and activating the P38 MAPK signaling pathway. Therefore, enhancing the expression of circST6GALNAC6 to promote ferroptosis or using circST6GALNAC6 as a biomarker of ferroptosis sensitivity is of considerable importance to the development and application of ferroptosis intervention methods in bladder cancer.

Laboratory Investigation (2022) 102:1323–1334; https://doi.org/10.1038/s41374-022-00826-3

INTRODUCTION

Bladder cancer is one of the most prevalent malignancies and a leading cause of cancer-related deaths in the world[1]. According to estimates from the American Cancer Society, bladder cancer accounted for ~4.4% of all cancer cases diagnosed in the United States, with an estimated 83,730 new diagnoses and 17,200 deaths in 2021[2]. Metastasis is the main cause of death in bladder cancer patients with a poor five-year survival rate of 8.1%[3]. No significant reduction in mortality in metastatic bladder cancer patients has been observed despite remarkable advances in radical cystectomy and adjuvant chemotherapy in recent decades[2]. Therefore, further understanding the molecular regulatory network of metastasis is necessary to develop precision treatment strategies for bladder cancer.

Recent evidence indicates a therapeutic effect of ferroptosis (a novel iron-dependent form of non-apoptotic cell death) on bladder cancer. Kong et al. reported that a natural product, baicalin, inhibits the progression of bladder cancer by inducing ferroptosis[4]. Ferroptosis caused by lipid peroxide accumulation also frequently occurred in recurrent bladder cancer after chemotherapy[5]. These findings suggest that determining the role of ferroptosis may provide a potential treatment for bladder cancer.

Circular RNA (circRNA), a new member of the family of non-coding RNA with unique covalently closed structures, was initially reported ~40 years ago[6,7]. circRNA was considered a useless genetic transcription of 'noise' for decades. However, with the rapid development of high-throughput sequencing technology, an increasing number of circRNA(s) have been shown to be dysregulated in tumor cells, suggesting that circRNA(s) may play an important role in the biological events of cancer cells, such as proliferation, metastasis and apoptosis[8–10]. Recent research indicates the possible involvement of circRNA in the regulation of ferroptosis in multiple cancers, such as gastric carcinoma, glioma and breast carcinoma[11–13].

Second-generation sequencing was performed in the previous study to screen differently expressed circRNAs between bladder cancer tissues and their pericarcinous tissues. The results show that circST6GAlNAC6 (derived from exon 5 of ST6GALNAC6 gene), with information comprising hsa_circ_0088708 from the circBase database (http://www.circbase.org/), was significantly reduced in bladder cancer tissues. Moreover, circST6GAlNAC6 is found mainly in the cytoplasm and acts as a negative regulation factor of bladder cancer cells by adsorption of miR-200[14]. This study describes the role of circRNA in bladder cancer, but its molecular basis is not well understood.

[1]Department of Thoracic Surgery, The Second Xiangya Hospital of Central South University, Changsha 410013 Hunan, PR China. [2]Hunan Key Laboratory of Early Diagnosis and Precise Treatment of Lung Cancer, The Second Xiangya Hospital of Central South University, Changsha 410013 Hunan, PR China. [3]Department of Urology, The Second Xiangya Hospital of Central South University, Changsha 410013 Hunan, PR China. ✉email: zhuxuan@csu.edu.cn

Received: 13 August 2021 Revised: 8 June 2022 Accepted: 4 July 2022
Published online: 9 August 2022

Heat shock proteins (HSPs) are a group of proteins produced by cells in response to stressful stimulates, such as heat shock, cold, hypoxia and pH shift[15]. HSPs normally act as molecular chaperones to protect cells from stressful conditions by stabilizing misfolded peptides, restoring denatured proteins or promoting their degradation. Evidence has shown an important role of HSPs in regulating tumor progression by controlling apoptosis and necrosis of tumor cells[16,17]. HSBP1, an important member of small HSPs, also known as HSP27 or HSP25, is highly inducible in human cervical cancer cells after erastin treatment (an inducer of ferroptosis) and prevented tumor cells from erastin-induced ferroptosis[18]. HSPB1 was significantly upregulated in bladder cancer[19]; thus, HSPB1 may be an important participant in bladder cancer cell ferroptosis. The P38 mitogen-activated protein kinase (MAPK) pathway can be activated by numerous environmental stimulants and regulates various cell processes, including survival, apoptosis and proliferation[20,21]. Several papers reported MAPK pathway involvement in ferroptosis[22–24], but no studies have revealed its relationship with HSPB1.

Herein, the overexpression of circST6GALNAC6 is reported to promote erastin-induced ferroptosis in vitro and in vivo. Mechanistically, circST6GALNAC6 bound to HSPB1 and reduced the phosphorylation of HSPB1, thereby inhibiting the activation of the HSPB1/ P38 MAPK signaling pathway and increasing the sensitivity of bladder cancer cells to ferroptosis. The current findings suggest that circST6GALNA6/HSBP1 might be a potential therapeutic axis for bladder cancer.

MATERIALS AND METHODS

Human bladder cancer specimen

Bladder cancer tissues from 30 diagnosed patients were obtained during surgery at The Second Xiangya Hospital of Central South University with their signed statement of informed consent. This study was also approved by the Ethics Committee of the Second Xiangya Hospital of Central South University. All tissues were immediately snap-frozen in liquid nitrogen and stored at −80 °C after surgery.

Bladder cancer cell lines and treatment

Human bladder carcinoma cell lines (UM-UC-3 and J82) were obtained from the Cell Bank of the Chinese Academy of Sciences (Shanghai, China). Cells grown in DMEM medium (Gibco, USA) containing fetal bovine serum (10%, Thermo Fisher Scientific) and penicillin/streptomycin (1%, Sigma, USA) were maintained in a cell incubator at 37 °C with 5% CO_2 at a constant humidity (95%). Where necessary, bladder cancer cells were incubated with erastin (MedChemExpress, USA), Ferrostatin-1 (MedChemExpress, USA), Deferoxamine (MedChemExpress, USA) or SB203580 (Selleck, USA) respectively.

circST6GALNAC6 (full-length) was cloned and inserted into the pLV-CMV-EF1-ZsGreen1-Puro vector (shortened to pLV-CMV) to establish circST6GALNAC6 over-expressed bladder cancer cell lines, and a scribble sequence was also inserted into pLV-CMV as negative control (circRNA-NC). The constructs were co-transfected into HEK293T cells in the presence of two helper vectors pSPAX2 and pMD2G to generate lentivirus, which was used to infect UM-UC-3 and J82 cells, respectively. After 24 h of infection or transfection, UM-UC-3 and J82 cells were harvested and treated with erastin (10 μM, Solarbio, China) for 24 h for subsequent experiments.

Full-length HSPB1, ΔN HSPB1 (with N-terminal deletion of HSPB1) and Ser-15 mutation (S15A) were inserted into pcDNA3.1 vector to construct UM-UC-3 and J82 cells over-expressing HSPB1. PKC expression vector PLV-CMV-PKC, its negative control PLV-CMV and specific shHSPB1 were purchased from Genema, Shanghai, China.

Quantitative real-time PCR (qRT-PCR) analysis

Total RNA was isolated from the treated UM-UC-3 and J82 cells by TRIzol (Invitrogen, USA), and the concentration of extracted RNA was measured using a NanoDrop 2000C spectrophotometer (Thermo Fisher Scientific, USA). Next, RNA was reverse-transcribed into cDNA using PrimeScript™ RT reagent Kit (Takara, Japan) according to the instruction of the manufacturers. Relative expression of circST6GALNAC6 was measured by AceQ Universal SYBR qPCR Master Mix (Vazyme, China) on an ABI 7500 PCR system (Applied Biosystems, USA) and analyzed using the $2^{-\Delta\Delta Ct}$ method. GAPDH was used as the internal control. The following primers are listed in Table 1.

Table 1. RT-qPCR primers in this study.

hcircST6GALNAC6	5′-ATTTGACGACCTCTTCCGGG-3′
	5′-TCTTGTTGCCCACATCAGCT-3′
SLC7A11	5′-TGACTGGAGTCCCTGCGTAT-3′
	5′-TGTTCTGGTTATTTTCTCCGACA-3′
GPX4	5′-TGGACGAGGGGAGGAGC-3′
	5′-GGGACGCGCACATGGT-3′
COX2	5′-CAAATTGCTGGCAGGGTTGC-3′
	5′-AGGGCTTCAGCATAAAGCGT-3′
GAPDH	5′-ATGACTCTACCCACGGCAAG-3′
	5′-CTGGAAGATGGTGATGGGTT-3′

Cell Counting Kit-8 (CCK-8) assay

The cell viability of UM-UC-3 and J82 cells was determined by the CCK-8 (Dojindo, Japan) method. The treated UM-UC-3 and J82 cells were simply inoculated onto a 96-well plate and replication holes were added. After incubation at 37 °C for 24 h, CCK-8 reagent was added to each well (10 μL per 100 μL medium) and then incubated for 2 h. The absorbance of each well was measured at 450 nm using a Varioskan Flash reader (Thermo Fisher Scientific, USA).

Western blot analysis

Proteins were isolated from treated UM-UC-3 and J82 cells or xenograft tumors using RIPA buffers (Thermo Fisher, USA). The 50 μg protein sample was separated by 10% SDS-PAGE after determining the protein concentration. The isolated proteins were then transferred onto a nitrocellulose membrane, followed by the incubation with 5% low-fat milk for 2 h. Afterwards, the membranes were incubated with indicated primary antibodies against SLC7A11 (1:1000, #12691, CST), GPX4 (1:2000, ab252833, Abcam), COX2 (1:1000, ab188183, Abcam), HSPB1 (1:1000, ab109376, Abcam), p-HSPB1 (1:2000, #2401, #2404, #2405, CST), p38 (1:2000, ab170099, Abcam), p-p38 (1:1000, ab178817, Abcam), JNK (1:500, ab199380, Abcam), p-JNK (1:500, ab124956, Abcam), PKC (1:500, ab181558, Abcam) and GAPDH (1:2000, ab8245, Abcam). After 24 h of incubation with indicated primary antibodies, the membranes were incubated with indicated secondary antibodies (Abcam) for 2 h, and the signals were examined by enhanced chemiluminescence reagent (EMD Millipore, USA).

Determination of lipid ROS, GSH and MDA levels

Treated UM-UC-3 and J82 cells were subjected to incubation with 2′,7′-dichlorofluorescein diacetate (BODIPY-C11, 50 mM, ABclonal) for 30 min to measure relative levels of lipid ROS. After washing with PBS three times, cellular fluorescence was examined using a fluorescence microscope (Olympus, Japan), and a CytoFLEX (BECKMAN, USA) was applied to determine the fluorescence intensity. Relative levels of GSH and MDA in the cell lysates of treated UM-UC-3 and J82 cells were evaluated by a GSH Colorimetric Detection Kit (CS0260, Sigma, USA) and lipid peroxidation (MDA) assay kit (ab118970, Abcam), respectively. The specific detection steps followed the instructions of the two kits.

Detection of cellular iron levels

Cellular iron levels were determined using phen green SK (PGSK) staining and confocal imaging of its fluorescence. In brief, treated UM-UC-3 and J82 cells were incubated with PGSK (5 μM, P14313, Molecular Probes, USA) for 20 min after washing with PBS twice. A fluorescence confocal microscope (Nikon, TSR, Japan) was then used to detect the fluorescence of cells in each group. The green fluorescence of PGSK was reduced in ferroptosis cells. In addition, the iron level of tumors in vivo was tested by Prussian Blue Iron Stain Kit (with Eosin solution, G1424, Solarbio, China).

CircRNA pull-down and mass spectrum analysis

Biotinylated circST6GALNA6 probe, which is designed and supplied by Genema (Shanghai, China), was heated at 95 °C for 5 min in PA buffer solution (Tri-HCl 10, $MgCl_2$ 10 and NH_4Cl 100 mM) and was then immobilized on MyOne Streptavidin C1 Dynabeads (Thermo Fisher, #65001). To prepare cell lysates, treated J82 cells (2×10^6) were collected and re-suspended in binding buffer (HEPES, 10 mM, KCl 50 mM, EDTA 1 mM, 10% glycerol and

105% Triton X-100). The supernatant was incubated with Dynabeads for 2 h after centrifugation at 13,000 RPM for 10 min. The beads were subsequently washed with PBS twice and boiled in Western blot sample buffer for 10 min. Half of the samples were then analyzed by mass spectrometry at the molecular biology core facility. Western blot analysis of HSPB1 protein was also performed on other specimens.

Fluorescence in situ hybridization (FISH) and immunofluorescence staining

The Cy5-tagged circST6GALNAC6 was designed and supplied by Genema (Shanghai, China). The treated UM-UC-3 and J82 cells were inoculated on coverslips and grown for 24 h and then fixed with 4% paraformaldehyde. Next, the cells were incubated overnight with a CY3-labeled circST6GALNAC6 probe (1:50) in PBS containing 0.5% Triton X-100. Afterwards, the cells were incubated with anti-HSPB1 (1:500, ab109376, Abcam) overnight, followed by the incubation with SYPRO Orange conjugated secondary antibody for 2 h. Signals were observed under a confocal microscope (Olympus, Japan).

RNA immunoprecipitation (RIP)

Treated UM-UC-3 and J82 cells were lysed in lysis buffer (Thermo Scientific, USA) containing RNase and protease inhibitors. Extracted proteins were incubated overnight with anti-HSPB1 (1:400, CST, USA) and then pulled down using a protein G Sepharose Fast Flow suspension (GE Amersham, UK). The beads were subjected to RNA purification using TRIzol reagent (Invitrogen) after 1 h of incubation with proteinase K.

Mouse xenografts

Nude mice (male, 7–8 weeks old) were provided by Hunan SJA Experimental Animal Co., LTD. The animal experiments were conducted in accordance with the guidelines of the Animal Experiment Ethics Committee of Central South University. J82 cells (2×10^5) stably expressing circrNA-NC or circST6GALNAC6 were implanted subcutaneously on the left side of nude mice ($n = 5$/group). After 7 days of inoculation, these mice were treated with erastin (1 mg/kg, thrice weekly) for 21 days, along with intratumoral injections of PLV-CMV-PKC and PLV-CMV-NC. The experiment was conducted with randomly selected littermates matched for sex, age and weight. The animals were then sacrificed by CO_2 asphyxiation at the specified time, and the tumors were resected and weighed. Half of the fresh xenograft tumors were lysed in RIPA buffer and subjected to Western blot analysis. The remaining tumor samples were fixed with 4% paraformaldehyde and cut into 5 μM sections for immunohistochemical analysis. Briefly, tumor slices were washed with PBS three times and incubated with normal donkey serum (20%, Sigma, USA) for 2 h in a vial. Afterwards, indicated primary antibodies against GPX4 (1:2000, ab252833, Abcam), COX2 (1:1000, ab188183, Abcam), p-HSPB1 (1:2000, #95357, CST) SLC7A11 (1:1000, #12691, CST or ab37185 for IHC) and were incubated overnight. Sections were incubated with HRP-conjugated secondary antibody (1:5000, ab205718, Abcam) for 2 h after washing with PBS twice. The cell proliferation of tumor sections was examined by the Ki-67 immunohistochemical Kit (YanJinbio, China).

Statistical analysis

Data in this study were expressed as mean ± standard deviation (Mean ± SE). GraphPad Prism (version 7.0) was used to collect and analyze data. Unpaired Student's *t* tests were employed to compare the means of two groups. A one-way (for one independent variable) or two-way (for two independent variables) analysis of variance with Tukey's multiple comparisons test was utilized for comparison amongst the different groups on all pairwise combinations. A two-tailed *P* value of <0.05 was considered statistically significant.

RESULTS

CircST6GALNAC6 increased ferroptosis in bladder cancer

The previous study indicated that circST6GAlNAC6 was transcribed and spliced from exon 5 of the ST6GALNAC6 gene, with full-length 407 nt (Supplementary Fig. S1). Kaplan–Meier survival analysis was performed, which indicated that the survival rate of bladder cancer patients with high circST6GALNAC6 expression was generally higher than that with low expression (Fig. 1A). CircST6GAlNAC6 was found mainly in the cytoplasm of bladder cancer cells (Fig. 1B), revealing that it can act as a 'protein sponge' or 'miRNA sponge'.

Two activators (erastin and RSL3) were used to induce ferroptosis at 0, 5, 10, 20, 50 and 100 μM for 24 h in several bladder cancer cell lines, including T24, J82, 5637, UM-UC-3 and SW780, to investigate the role of circST6GALNAC6 in ferroptosis. Cell viabilities were analyzed by CCK-8 assay and were decreased in an erastin or RSL3 dose-dependent manner (Supplementary Fig. S2A), However, RSL3 treatment did not induce the circST6GALNAC6 expression as much as erastin did (Fig. 1C). This finding suggests that circST6GALNAC6 might only be associated with mitochondria ROS-dependent ferroptosis, which was induced by erastin but not RSL3.

Erastin primarily induces ferroptosis by influencing mitochondrial voltage-dependent anionic channels. Thus, the mitochondrial morphology of bladder cancer cells was examined by intracellular electron microscopy. We saw more atypical morphology (small volume, inner crest ablation and deepened matrix density) in the circST6GALNAC6 overexpression group compared to the NC group under erastin processing (Supplementary Figs. S2B and S3). In addition, the cell viability of J82 and UM-UC-3 was significantly decreased after erastin treatment and further reduced after circST6GALNAC6 overexpression (Fig. 1D). The mRNA and protein levels of ferroptosis-related proteins (SLC7A11, GPX4) were dramatically decreased whilst COX2 increased during erastin-induced ferroptosis, and circST6GALNAC6 further enhanced the significance of changes in the expression of these indicators (Fig. 1E, F). Lipid ROS, malondialdehyde (MDA), glutathione (GSH) and iron (Fe^{2+}) levels were also altered after erastin and circST6GALNAC6 overexpression (Fig. 1G–J), suggesting that circST6GALNAC6 overexpression increased ferroptosis in bladder cancer cell lines.

Next, ferroptosis inhibitors Fer-1 and deferoxamine were added respectively in the circST6GALNAC6-OE cells with or without the presence of erastin. The results show that both inhibitors attenuated the effect of circST6GALNAC6 on ferroptosis, which was reflected in the recovery of cell viability, protein levels of ferroptosis-related proteins (GPX4, SLC7A11, COX2 and GSH) and the reduction of MDA, lipid ROS and Fe^{2+} content (Supplementary Figs. S4A–F).

HSPB1 bound to circST6GALNA6 in bladder cancer

Mass spectrometry analysis was performed on circST6GALNAC6 pull-down proteins that were determine by silver staining of circST6GALNAC6-OE cells (Fig. 2A, B), to explore the ferroptosis regulation mechanism of circST6GALNAC6. Gene ontology analysis showed that these proteins were closely correlated with several pathways, such as VEGF, apoptosis and RAS pathways (Fig. 2C). HSPB1, a critical member of the VEGF signaling pathway, was found to be highly enriched in the circST6GALNAC6-OE cells compared with NC (Fig. 2D–G). Considering its role in ferroptosis resistance in cancer cells[18], the role of circST6GALNAC6 in regulating bladder cancer ferroptosis via HSPB1 remains unclear.

Erastin enhanced binding of circST6GALNAC6 and HSPB1 in bladder cancer

FISH and immunofluorescence analysis, RNA immunoprecipitation (RIP) and RNA pull-down assays were performed to verify the binding relationship between circST6GALNAC6 and HSPB1. More HSPB1 was obtained with the circST6GALNAC6 probe in the presence of erastin than that in its absence (Fig. 3A–D).

The binding domain of circST6GALNAC6 in HSPB1 was further explored. The loss of the N-terminal domain with concentrated phosphorylation sites led to failure of circST6GALNAC6 to bind HSPB1 (Fig. 3E, F). CircST6GALNAC6 overexpression significantly inhibited the phosphorylation level of HSPB1 in the Ser-15 site and has no significant influence on Ser-78 or Ser-82 sites (Fig. 3G). These results indicate that circST6GALNAC6 binds efficiently to the N-terminal domain of HSPB1 and inhibits the phospho-activation at the Ser-15 site, which is induced under the stress of ferroptosis.

PKC was then used to activate HSPB1 phosphorylation. When circST6GALNAC6 was overexpressed, PKC was added to determine whether circST6GALNAC6-mediated phospho-inhibition at Ser-15

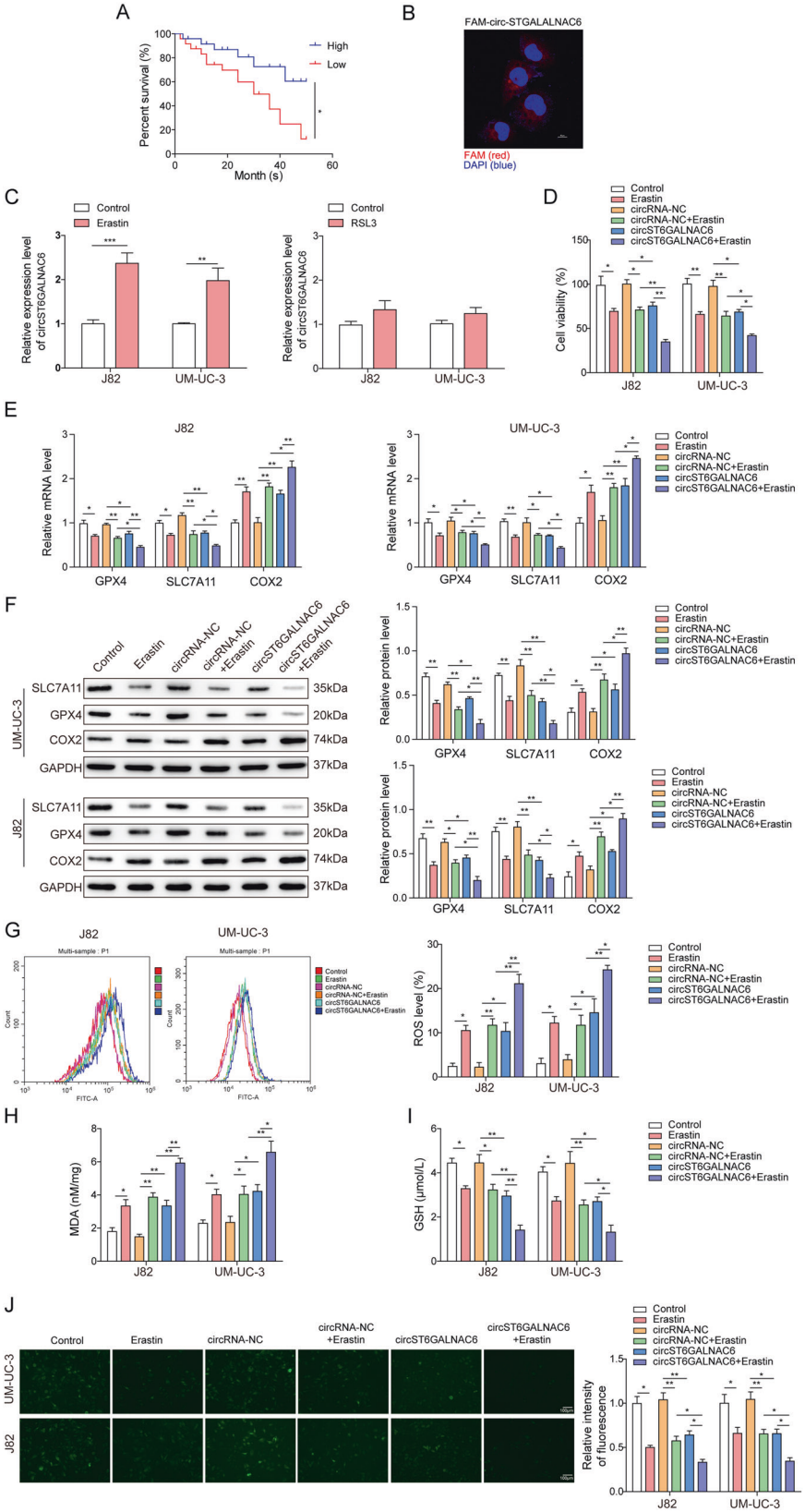

site was reversed by PKC, thus producing the opposite effect from p-HSPB1 on ferroptosis in bladder cancer cells. Data from cell viability, ferroptosis-related proteins, including HSPB1 and p-HSPB1 expression and lipid ROS, Fe2+, MDA and GSH all supported that circST6GALNAC6 diminished the phosphorylation level of HSPB1 and increase ferroptosis sensitivity in bladder cancer (Fig. 4A–G).

Subsequent studies examined the effects on bladder cancer cell ferroptosis when HSPB1 was over-expressed or knocked down.

Fig. 1 CircST6GALNAC6 increased the sensitivity of bladder cancer cells to ferroptosis. A Kaplan–Meier survival analysis was performed to analyze the survival rate of bladder cancer patients with low and high expressions of circST6GALNAC6. **B** Cellular location of circST6GALNAC6 in J82 cell line. **C** J82 and UM-UC-3 cells were subjected to the detection of circST6GALNAC6 expression by qRT-PCR after treatment with erastin for 24 h. **D** J82 and UM-UC-3 cells were transfected with circST6GALNAC6 over-expressed plasmid or negative control plasmid and treated with erastin for 24 h. Cell viability of treated J82 and UM-UC-3 cells was determined by CCK-8 assay. **E** qRT-PCR and **F** Western blot assays were employed to measure the expression of ferroptosis-related proteins at mRNA and protein levels, respectively, in treated J82 and UM-UC-3 cells. **G** ROS production of J82 and UM-UC-3 cells after treatment was analyzed by Bodipy-C11 staining and flow cytometry. **H** MDA and **I** GSH levels in the cell lysates of treated UM-UC-3 and J82 cells were detected by commercial kits. **J** Intracellular iron level in treated J82 and UM-UC-3 cells was determined by fluorescent indicator PGSK. The mean ± SD in the graph shows the relative levels from three replicates. $*p < 0.05$, $**p < 0.01$.

Firstly, a full-length HSPB1 wild-type expression vector, △N-terminal expression vector, shHSPB1 and shRNA interference vector (Supplementary Fig. S5) were constructed, and bladder cancer cells were then transfected with these vectors with or without erastin. Ferroptosis in each group was tested by the experimental methods as in the previous study. The results indicated that the circST6GALNAC6 binding N-terminal domain was the main functional unit of HSPB1 to exert ferroptosis stress resistance in bladder cancer and was dependent on phospho-Ser-15, which was significantly inhibited during circST6GALNAC6 overexpression. This section concludes that HSPB1 phosphorylation inhibition was related to the space-occupying effect caused by circST6GALNAC6 binding and therefore significantly affected ferroptosis in bladder cancer (Fig. 5A and H and Supplementary Fig. S6).

CircST6GALNAC6/HSPB1 axis regulated bladder cancer cell ferroptosis through the p38 MAPK pathway

Potential downstream signaling pathways of the circST6GALNAC6/HSPB1 axis were determined to identify the execution route in bladder cancer ferroptosis. Results indicated that the protein levels of p-p38 MAPK and p-JNK were notably increased in the circST6GALNAC6-OE group during erastin-induced ferroptosis, which was abolished either by the overexpression of HSPB1 or treatment of cells with PKC (Fig. 6A). P38 inhibitors or HSPB1 overexpression in erastin treatment significantly increased the survival rate of circST6GALNAC6-OE cells (Fig. 6B). In addition, the levels of lipid ROS, MDA, Fe^{2+} and COX2 decreased, and SLC7A11, GPX4 and GSH increased (Fig. 6C–G), suggesting that ferroptosis in bladder cancer cells was effectively facilitated through CircST6GALNAC6/HSPB1/p38 MAPK pathway.

In vivo validation of the role of circST6GALNA6/HSPB1/p38 AMPK axis in regulating bladder cancer cell ferroptosis

The regulatory effects of circST6GALNA6/HSPB1/p38 AMPK axis on bladder cancer cell ferroptosis were further tested in vivo in a nude mouse model transplanted with circST6GALNA6 over-expressed J82 cells. Results showed that circST6GALNAC6 overexpression enhanced the repressive effects of erastin on tumor volume (Fig. 7A) and weight (Fig. 7B), whilst this phenomenon was not observed in the PKC treated group. The expression of SLC7A11, GPX4, COX2 and p-HSPB1 in the xenograft tumors in each group was also assessed by Western blot. The promotion of erastin-induced SLC7A11, GPX4 reduction and the increase in COX2 by circST6GALNAC6 overexpression in the PKC group were reversed (Fig. 7C). Consistent with the results in vitro, circST6GALNAC6 inhibited the phosphorylation level of HSPB1, which was partially rescued by PKC overexpression (Fig. 7D). PKC treatment also abolished the enhanced effects of circST6GALNAC6 overexpression on the erastin-induced MDA upregulation and GSH downregulation in the xenograft tumors (Fig. 7E, F, respectively). Erastin increased the protein expression levels of p-p38 and p-JNK, which were both further enhanced or blocked by circST6GALNAC6 or PKC overexpression (Fig. 7G). Immunohistochemical (IHC) and iron staining methods were eventually conducted to assess the expression of SLC7A11, GPX4 and iron content in each group, which showed that the decreased levels of GPX4 and SLC7A11 and the increased levels of iron due to circST6GALNAC6 overexpression were partially avoided under the extra PKC treatment (Fig. 7H, I). RNA pull-down and RIP-PCR assays were performed to further evaluate the interaction of circST6GALNAC6 and HSPB1 in vivo, and both results suggested that circST6GALNAC6 can bind to HSPB1 (Supplementary Fig. S7A, B). Overall, these findings supported that circST6GALNAC6 increased bladder cancer cells to ferroptosis by decreasing the phosphorylation level of HSPB1 in vivo.

DISCUSSION

The extreme stability, high abundance and tissue-specific expression of circRNA(s) in human cancer make them a promising biomarker and target for cancer diagnosis and treatment[25]. Thus, circRNA(s) play critical roles in regulating various cellular events of cancer cells[25]. Recent reports indicate that circRNA(s) are one of the key mediators in regulating cancer cell ferroptosis. For instance, circ_0008035 was revealed to be an 'oncogene' that represses gastric cancer cell ferroptosis through the miR-599/EIF4A1 axis[11]. Circ_ABCB10 helped increase ferroptosis sensitivity in rectal cancer cells[26]. Circ_IL4R facilitated the tumorigenesis and repressed ferroptosis of hepatocellular carcinoma[27]. Different circRNA(s) have various effects and regulation mechanisms on ferroptosis. Therefore, the relationship between circRNA(s) and ferroptosis merits investigation.

The current study shows, for the first time, that circST6GALNAC6 enhanced the sensitivity of bladder cancer cells to erastin-induced ferroptosis by interacting with HSPB1 in vivo and in vitro, Therefore, induction of ferroptosis by controlling the circST6GALNAC6/HSPB1/P38 regulatory axis might be a new therapeutic option for bladder cancer.

HSPB1 is widely expressed in a variety of tumor tissues, and high expression of HSPB1 is closely associated with poor prognosis[28]. In BC, HSPB1 is closely related to tumor grade, clinical stage, DNA ploidy and recurrence, and its expression has a statistically significant impact on the survival of bladder cancer patients[29]. Herein, changes in total HSPB1 protein level were absent in the circST6GALNAC6 overexpression group compared with the control group. However, circST6GALNAC6 overexpression significantly reduced the phosphorylation level of HSPB1 and promoted ferroptosis. These findings are consistent with previous ones that indicated the contribution of HSPB1 phosphorylation to ferroptosis[18].

Bioinformatics (RNA-Protein Interaction Prediction, RPISeq) indicated that the most likely circST6GALNAC6 binding domain of HSPB1 is the N-terminal, where three common phosphorylation sites are found (Ser-15, Ser-78 and Ser-82)[30]. Thus, the binding of circST6GALNAC6 to the N-terminal domain of HSPB1 might lead to the inactivation of these possible phosphorylation sites through space occupation (Fig. 7J).

The results of this study showed that erastin increased the expression of p-HSPB1 (Ser-15, Ser-78 and Ser-82), but only the Ser-15 phosphorylation site was diminished by circST6GALNAC6 binding, thus relieving the inhibitory effects of HSPB1 on ferroptosis. The N-terminus of HSPB1 was deleted to further confirm the binding domain of circST6GALNAC6 in HSPB1. The findings revealed that circST6GALNAC6 did not bind to HSPB1, and the effect of circST6GALNAC6 on the bladder cancer ferroptosis was eliminated. All the above results suggested that circST6GALNAC6 binds to the N-terminus of HSPB1.

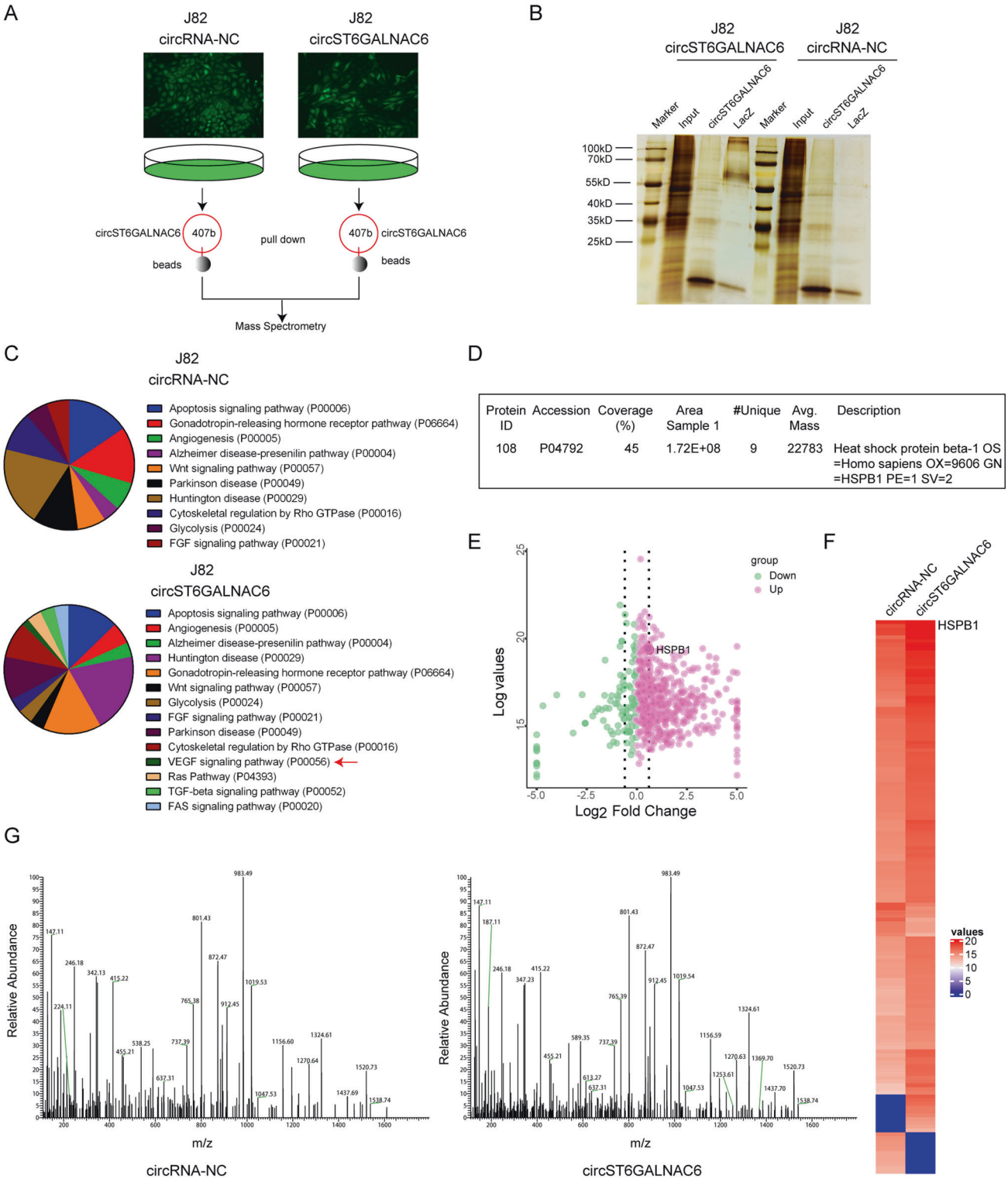

Fig. 2 Identification of circST6GALNA6-binding proteins. A Schematic of the method. J82 cells with stable expression of CircRNA-NC or circST6GALNAC6 were pulled down using agarose beads, and the supernatant was analyzed by quantitative mass spectrometry after thorough washing. **B** The circST6GALNA6-related proteins were determined using silver staining. **C** Gene Ontology analysis of the dysregulated proteins in circST6GALNAC6 over-expressed group in J82 cells. **D** A summary of peptide masses matching with theoretical peptide masses of HSPB1. **E** Volcano plot map showing the proteins pulled down by circST6GALNAC6 probe, wherein HSPB1 protein has been marked. **F** Heat map showing the proteins pulled down by circST6GALNAC6 probe. **G** Peaks of peptide masses corresponding to HSPB1 peptide fragments. The mean ± SD in the graph shows the relative levels from three replicates. $*p < 0.05$, $**p < 0.01$.

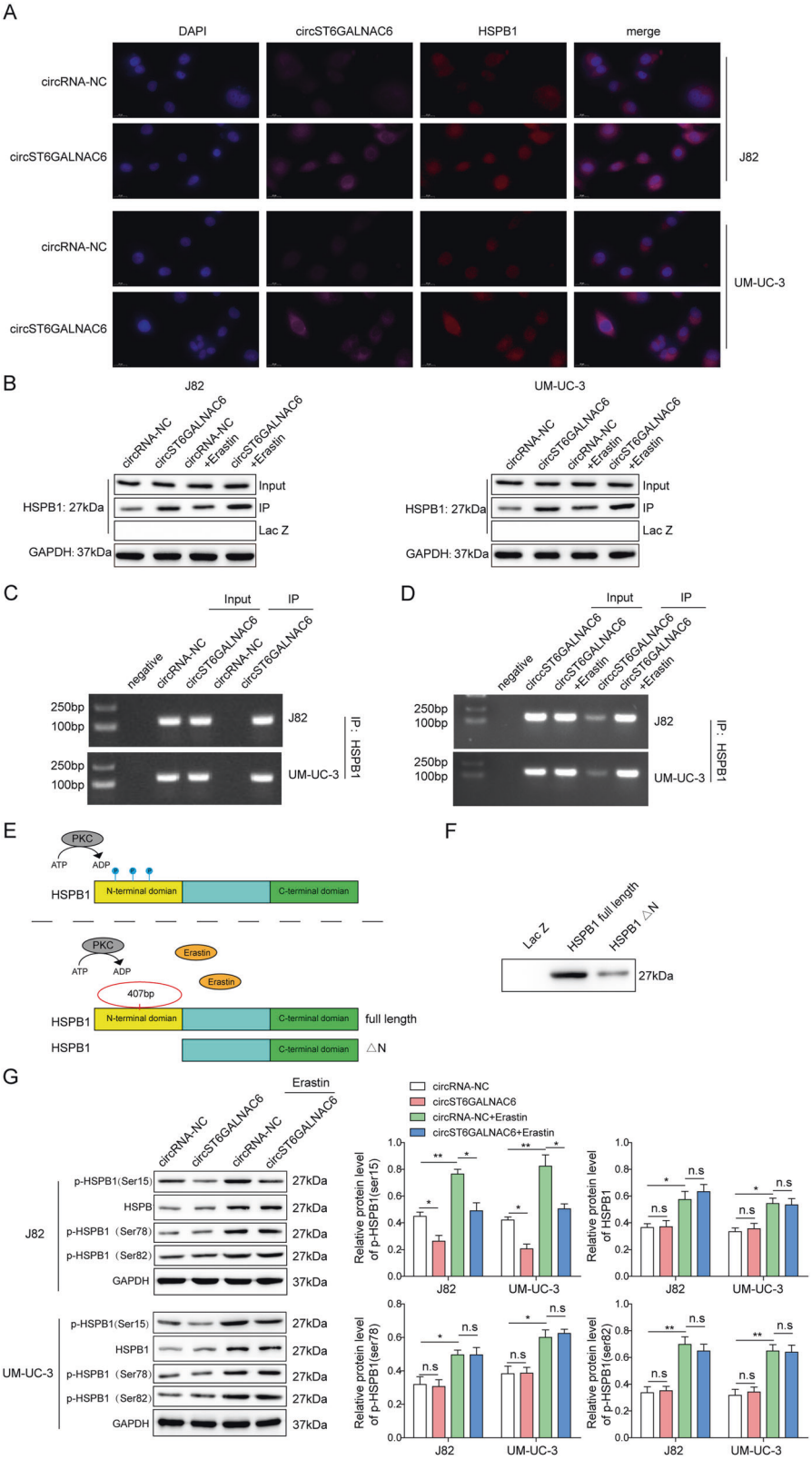

Fig. 3 Erastin promoted the binding of circST6GALNAC6 and HSPB1 in bladder cancer. A Immunofluorescence double staining showed that circST6GALNAC6 and HSPB1 were co-located in J82 and UM-UC-3 cells, respectively. **B** RNA pull-down and **C**, **D** RIP assays were used to determine the interaction between circST6GALNAC6 and HSPB1 in J82 and UM-UC-3 cells with or without erastin. **E** A proposed model of the relationship between circST6GALNAC6 and HSPB1. **F** RNA pull-down assay was used to study the circST6GALNAC6 binding sites in the HSPB1 protein. **G** Western blot analysis of p-HSPB1 level in J82 and UM-UC-3 cells transfected with circST6GALNAC6 or circRNA-NC in the presence of protein kinase C and erastin. The mean ± SD in the graph shows the relative levels from three replicates. $^{*}p < 0.05$, $^{**}p < 0.01$.

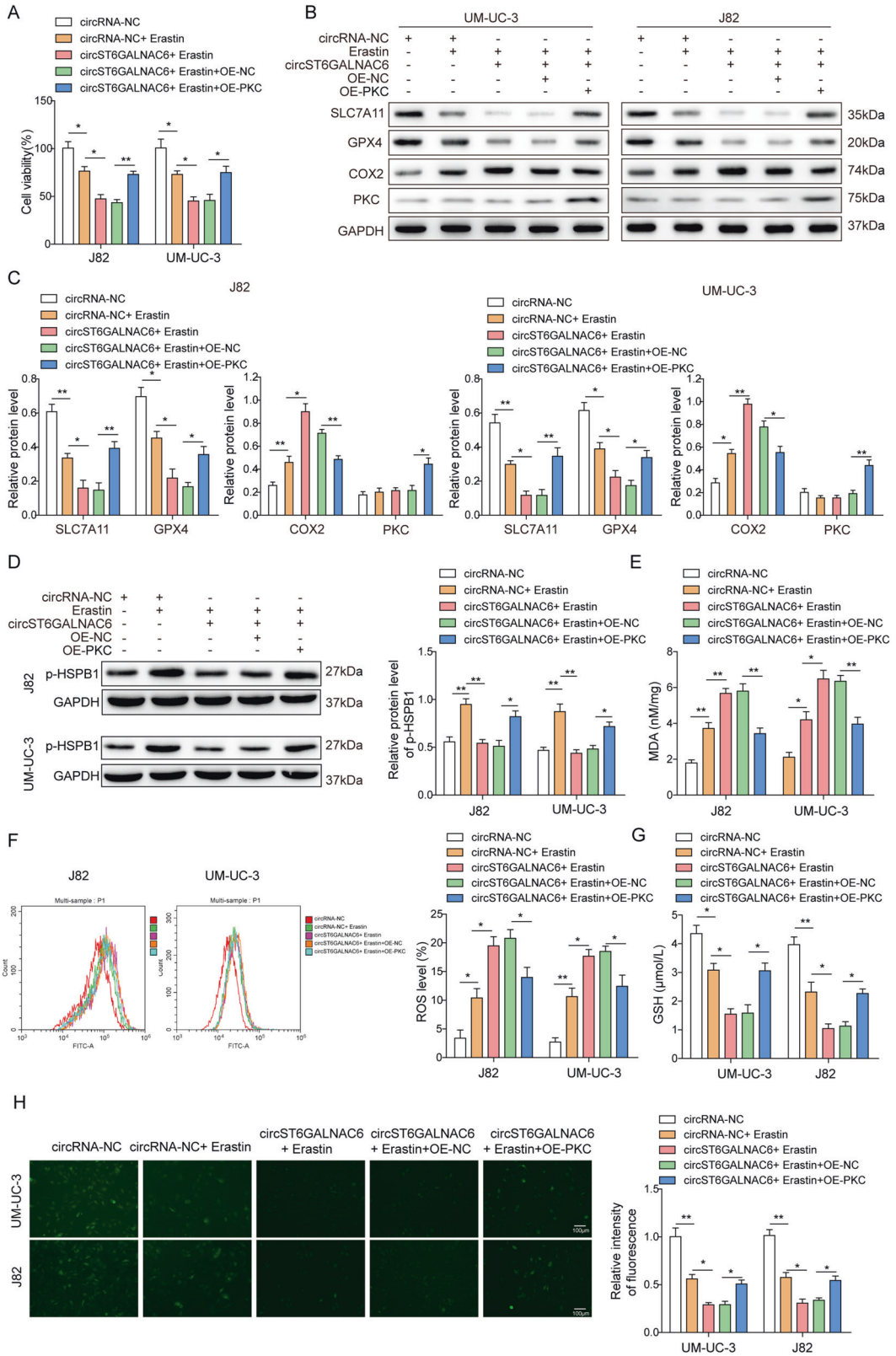

Fig. 4 CircST6GALNAC6 increased the sensitivity of bladder cancer cells to ferroptosis by binding HSPB1. J82 and UM-UC-3 cells were transfected with circST6GALNAC6 overexpression plasmid or/and OE-PKC and then treated with erastin for 24 h. **A** CCK-8 assay was adopted to test the cell viability of treated UM-UC-3 and J82 cells. **B**–**D** The protein expression of SLC7A11, GPX4, COX2, p-HSPB1 and PKC in treated J82 and UM-UC-3 cells was measured by Western blot. Productions of (**E**) MDA, (**F**) ROS and (**G**) GSH in treated J82 and UM-UC-3 cells were assayed. **H** Intracellular iron level in treated J82 and UM-UC-3 cells was determined by fluorescent indicator PGSK. The mean ± SD in the graph shows the relative levels from three replicates. $^{*}p < 0.05$, $^{**}p < 0.01$.

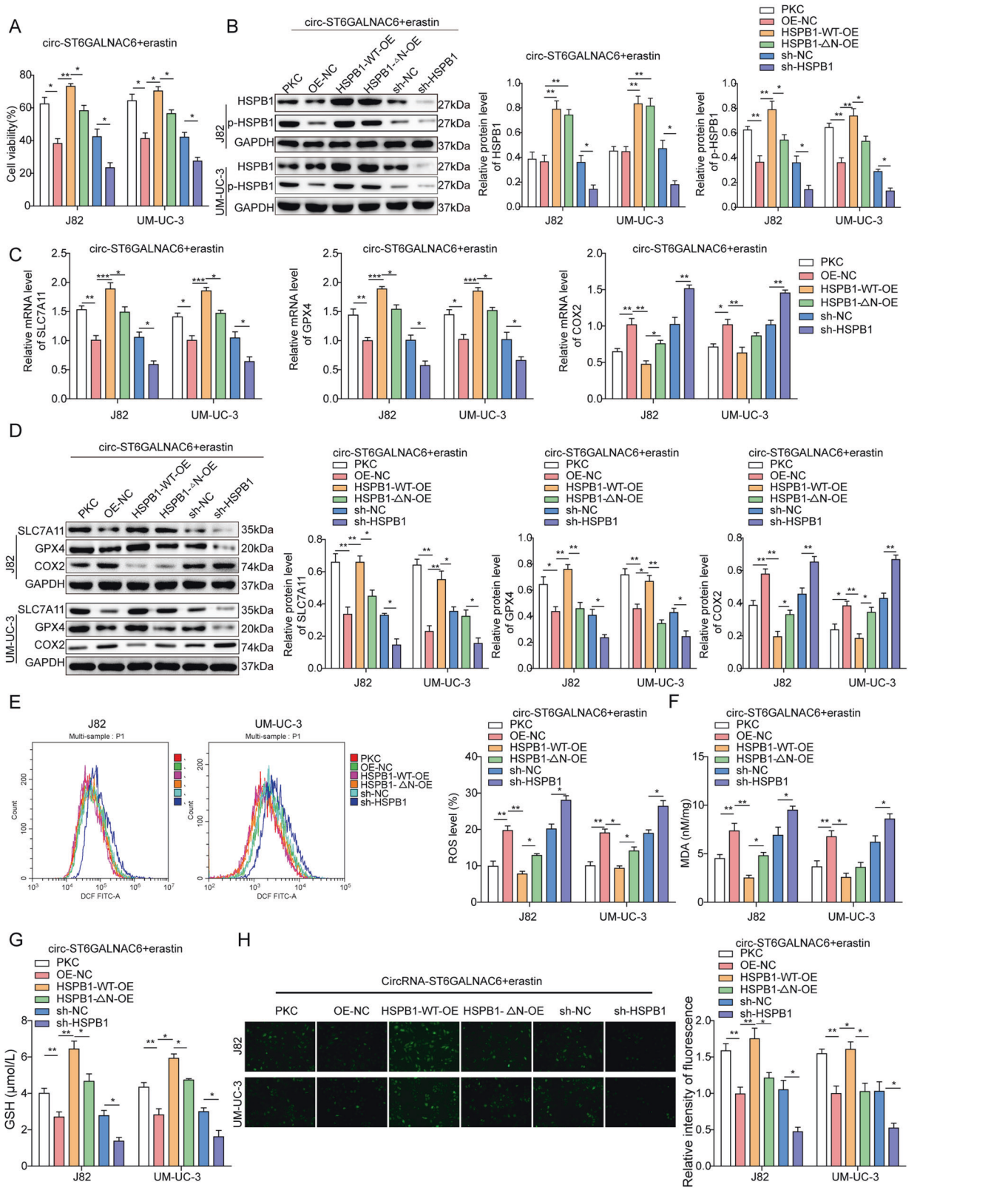

Fig. 5 HSPB1 N-terminal interacted with circST6GALNAC6 and mediated its effects on bladder cancer cell ferroptosis. A CCK-8 assay was adopted to evaluate cell viability after treatment with circST6GALNAC6 and OE-PKC, OE-NC, HSPB1-WT-OE, HSPB1-△N-OE, sh-NC or sh-HSPB1 in the presence of erastin. **B** Protein levels of HSPB1 and p-HSPB1 were detected in cells treated as indicated in the presence of erastin. **C**, **D** qRT-PCR and Western blot were employed to evaluate the expression of SLC7A11, GPX4 and COX2 in cells treated as indicated in the presence of erastin. Production of (**E**) ROS, (**F**) MDA and (**G**) GSH were measured in cells treated as indicated in the presence of erastin. **H** Intracellular iron level in treated cells was determined by fluorescent indicator PGSK. The mean ± SD in the graph shows the relative levels from three replicates. $^{*}p < 0.05$, $^{**}p < 0.01$.

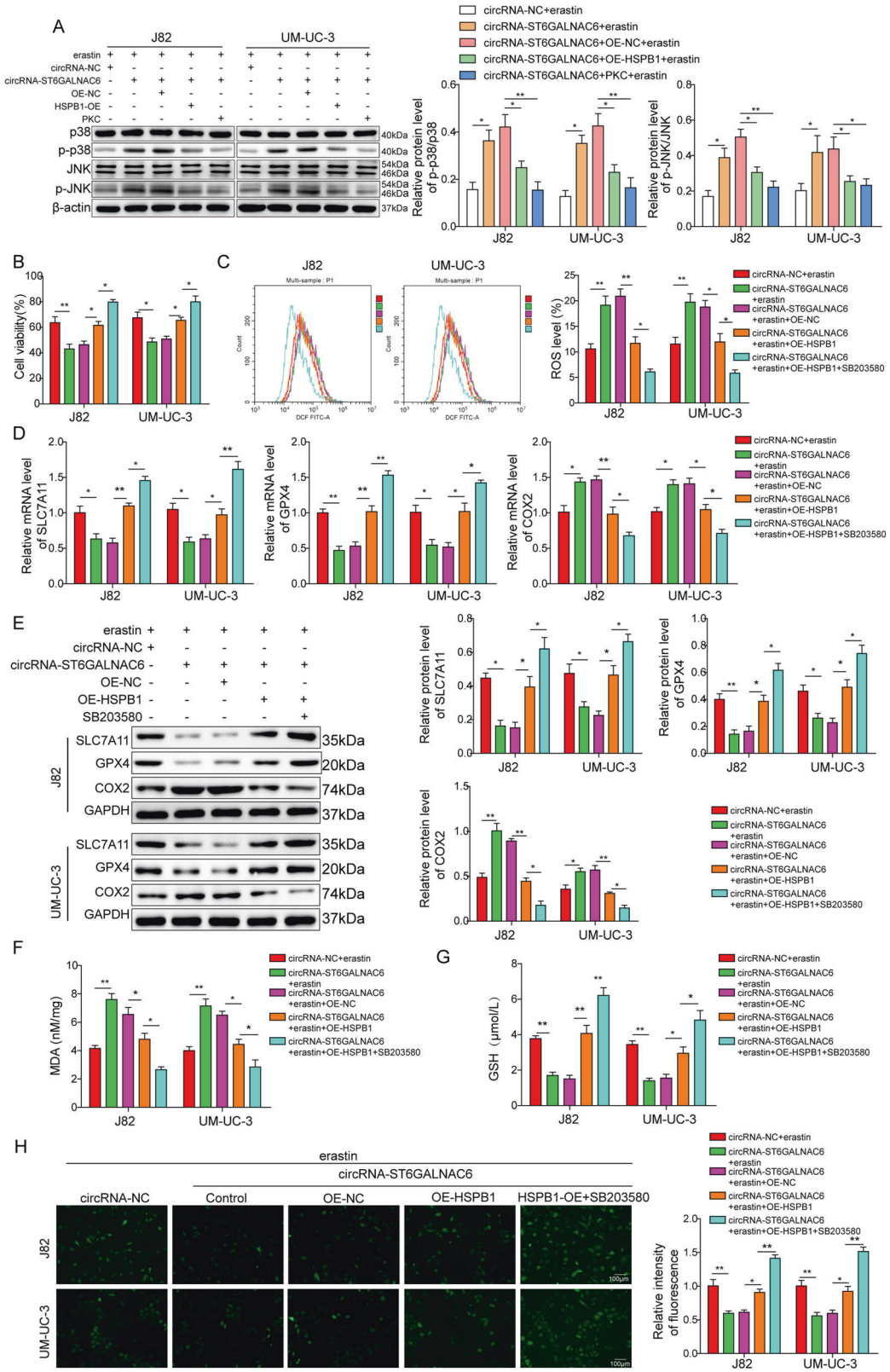

Fig. 6 CircST6GALNAC6/HSPB1 axis regulated bladder cancer cell ferroptosis sensitivity through the p38 MAPK pathway. A Protein levels of p38, p-p38, JNK and p-JNK were detected in circST6GALNAC6 over-expressed cells treated with HSPB1-OE in the presence of erastin. **B** CCK-8 analysis of cell viability in circST6GALNAC6 over-expressed cells treated with HSPB1-OE in the presence of erastin with or without the p38 inhibitor. **C** ROS level in circST6GALNAC6 over-expressed cells treated with HSPB1-OE in the presence of erastin with or without the p38 inhibitor. **D**, **E** qRT-PCR and Western blot analysis of SLC7A11, GPX4 and COX2 in circST6GALNAC6 over-expressed cells in the presence of erastin after treatment with HSPB1-OE with or without the p38 inhibitor. **F**, **G** Production of MDA and GSH in circST6GALNAC6 over-expressed cells in the presence of erastin after treatment with HSPB1-OE with or without the p38 inhibitor. **H** Intracellular iron level in treated cells was determined by fluorescent indicator PGSK. The mean ± SD in the graph shows the relative levels from three replicates. $^{*}p < 0.05$, $^{**}p < 0.01$.

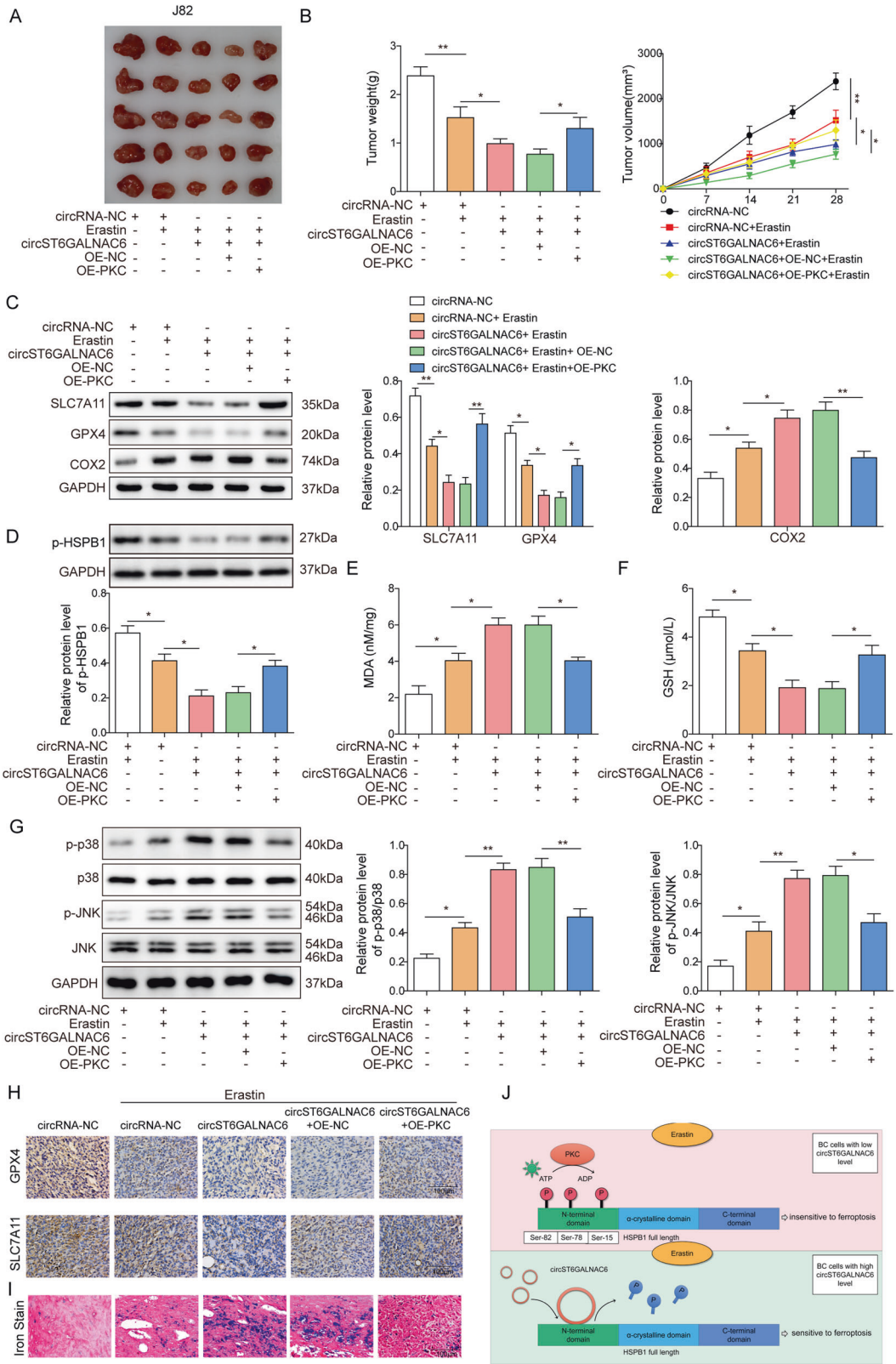

Fig. 7 Role of the circST6GALNA6/HSPB1 axis in regulating bladder cancer cell ferroptosis was validated in vivo. J82 cells stably expressed circST6GALNAC6 or/and OE-PKC were delivered into the left flank of nude mice. Mice were treated with erastin (1 mg/kg) for 21 days after 7 days of inoculation. Tumors were removed, photographed and weighted at the end of the experiment. **A** Representative images of tumors from each group were shown. **B** Tumor volume and growth curve. **C**, **D** The protein expressions of SLC7A11, GPX4, COX2 and p-HSPB1 in the tumors from each group were detected. The production of (**E**) MDA and (**F**) GSH in the tumors from each group was assayed. **G** The protein expressions of p-p38, p38, p-JNK and JNK in the tumors from each group were detected. **H** Immunohistochemical analysis of Ki67, SLC7A11, GPX4 and p-HSPB1 in the tumors from each group. **I** Iron stain in the tumors from each group. **J** A graphical model of the conclusion. The mean ± SD in the graph shows the relative levels from three replicates. *$p < 0.05$, **$p < 0.01$.

Overall, this study clarified the possible regulatory mechanism of circST6GALNAC6 in bladder cancer cell ferroptosis. CircST6GALNAC6 increased the sensitivity of bladder cancer cells to erastin-induced ferroptosis through binding to the vicinity of the Ser-15 site of HSPB1 and blocking its phosphorylation. This mechanism partially depended on the phosphorylation repression of HSPB1 under ferroptosis stress. To date, few studies have reported that circRNA(s) affects ferroptosis by binding HSPs. The cellular stress response is a complex network. Thus, HSPB1 phosphorylation induced by erastin may be the beginning of a cascade, which deserves further in-depth study.

DATA AVAILABILITY

All data generated or analyzed during this study are included in this published article.

REFERENCES

1. Martinez Rodriguez, R. H., Buisan Rueda, O. & Ibarz, L. Bladder cancer: present and future. *Med Clin* **149**, 449-455 (2017).
2. Siegel, R. L., Miller, K. D., Fuchs, H. E. & Jemal, A. Cancer Statistics, 2021. *CA Cancer J Clin* **71**, 7-33 (2021).
3. Abdollah, F., Gandaglia, G., Thuret, R., Schmitges, J., Tian, Z., Jeldres, C. et al. Incidence, survival and mortality rates of stage-specific bladder cancer in United States: a trend analysis. *Cancer Epidemiol* **37**, 219-225 (2013).
4. Kong, N., Chen, X. Y., Feng, J., Duan, T., Liu, S. P., Sun, X. N. et al. Baicalin induces ferroptosis in bladder cancer cells by downregulating FTH1. *Acta Pharm Sin B* **11**, 4045-4054 (2021).
5. Qi, A., Wang, C., Ni, S., Meng, Y., Wang, T., Yue, Z. et al. Intravesical Mucoadhesive Hydrogel Induces Chemoresistant Bladder Cancer Ferroptosis through Delivering Iron Oxide Nanoparticles in a Three-Tier Strategy. *ACS Appl Mater Interfaces*, **13**, 44 (2021).
6. Hsu, M. T. & Coca-Prados, M. Electron microscopic evidence for the circular form of RNA in the cytoplasm of eukaryotic cells. *Nature* **280**, 339-340 (1979).
7. Cocquerelle, C., Mascrez, B., Hetuin, D. & Bailleul, B. Mis-splicing yields circular RNA molecules. *FASEB J* **7**, 155-160 (1993).
8. Memczak, S., Jens, M., Elefsinioti, A., Torti, F., Krueger, J., Rybak, A. et al. Circular RNAs are a large class of animal RNAs with regulatory potency. *Nature* **495**, 333-338 (2013).
9. Rybak-Wolf, A., Stottmeister, C., Glazar, P., Jens, M., Pino, N., Giusti, S. et al. Circular RNAs in the Mammalian brain are highly abundant, conserved, and dynamically expressed. *Mol Cell* **58**, 870-885 (2015).
10. Lei, M., Zheng, G., Ning, Q., Zheng, J. & Dong, D. Translation and functional roles of circular RNAs in human cancer. *Mol Cancer* **19**, 30 (2020).
11. Li, C., Tian, Y., Liang, Y. & Li, Q. Circ_0008035 contributes to cell proliferation and inhibits apoptosis and ferroptosis in gastric cancer via miR-599/EIF4A1 axis. *Cancer Cell Int* **20**, 84 (2020).
12. Zhang, H. Y., Zhang, B. W., Zhang, Z. B. & Deng, Q. J. Circular RNA TTBK2 regulates cell proliferation, invasion and ferroptosis via miR-761/ITGB8 axis in glioma. *Eur Rev Med Pharmacol Sci* **24**, 2585-2600 (2020).
13. Zhang, H., Ge, Z., Wang, Z., Gao, Y., Wang, Y., Qu, X. Circular RNA RHOT1 promotes progression and inhibits ferroptosis via mir-106a-5p/STAT3 axis in breast cancer. *Aging (Albany NY)* **13**, 8115-8126 (2021).
14. Tan, S., Kang, Y., Li, H., He, H. Q., Zheng, L., Wu, S. Q. et al. circST6GALNAC6 suppresses bladder cancer metastasis by sponging miR-200a-3p to modulate the STMN1/EMT axis. *Cell Death Dis* **12**, 168 (2021).
15. Saini, J. & Sharma, P. K. Clinical, prognostic and therapeutic significance of heat shock proteins in cancer. *Curr Drug Targets* **19**, 1478-1490 (2018).
16. Takayama, S., Reed, J. C. & Homma, S. Heat-shock proteins as regulators of apoptosis. *Oncogene* **22**, 9041-9047 (2003).
17. Rogalla, T., Ehrnsperger, M., Preville, X., Kotlyarov, A., Lutsch, G., Ducasse, C. et al. Regulation of Hsp27 oligomerization, chaperone function, and protective activity against oxidative stress/tumor necrosis factor alpha by phosphorylation. *J Biol Chem* **274**, 18947-18956 (1999).
18. Sun, X., Ou, Z., Xie, M., Kang, R., Fan, Y., Niu, X. et al. HSPB1 as a novel regulator of ferroptotic cancer cell death. *Oncogene* **34**, 5617-5625 (2015).
19. Kamada, M., So, A., Muramaki, M., Rocchi, P., Beraldi, E., Gleave, M. Hsp27 knockdown using nucleotide-based therapies inhibit tumor growth and enhance chemotherapy in human bladder cancer cells. *Mol Cancer Ther* **6**, 299-308 (2007).
20. Wada, T. & Penninger, J. M. Mitogen-activated protein kinases in apoptosis regulation. *Oncogene* **23**, 2838-2849 (2004).
21. Arthur, J. S. & Ley, S. C. Mitogen-activated protein kinases in innate immunity. *Nat Rev Immunol* **13**, 679-692 (2013).
22. Chang, W. T., Bow, Y. D., Fu, P. J., Li, C. Y., Wu, C. Y., Chang, Y. H. et al. A marine terpenoid, heteronemin, induces both the apoptosis and ferroptosis of hepatocellular carcinoma cells and involves the ROS and MAPK pathways. *Oxid Med Cell Longev* **2021**, 7689045 (2021).
23. Li, L., Hao, Y., Zhao, Y., Wang, H., Zhao, X. Jiang, Y. et al. Ferroptosis is associated with oxygen-glucose deprivation/reoxygenation-induced Sertoli cell death. *Int J Mol Med* **41**, 3051-3062 (2018).
24. Li, Y., Chen, F., Chen, J., Chan, S., He, Y., Liu, W. et al. Disulfiram/copper induces antitumor activity against both nasopharyngeal cancer cells and cancer-associated fibroblasts through ROS/MAPK and ferroptosis pathways. *Cancers* **12**, 138 (2020).
25. Kristensen, L. S., Hansen, T. B., Veno, M. T. & Kjems, J. Circular RNAs in cancer: opportunities and challenges in the field. *Oncogene* **37**, 555-565 (2018).
26. Xian, Z. Y., Hu, B., Wang, T., Cai, J. L., Zeng, J. Y., Zou, Q. et al. CircABCB10 silencing inhibits the cell ferroptosis and apoptosis by regulating the miR-326/CCL5 axis in rectal cancer. *Neoplasma* **67**, 1063-1073 (2020).
27. Xu, Q., Zhou, L., Yang, G., Meng, F., Wan, Y., Wang, L. et al. CircIL4R facilitates the tumorigenesis and inhibits ferroptosis in hepatocellular carcinoma by regulating the miR-541-3p/GPX4 axis. *Cell Biol Int* **44**, 2344-2356 (2020).
28. Nagaraja, G. M., Kaur, P. & Asea, A. Role of human and mouse HspB1 in metastasis. *Curr Mol Med* **12**, 1142-1150 (2012).
29. El-Meghawry El-Kenawy, A., El-Kott, A. F. & Hasan, M. S. Heat shock protein expression independently predicts survival outcome in schistosomiasis-associated urinary bladder cancer. *Int J Biol Markers* **23**, 214-218 (2008).
30. Zhang, D., Wong, L. L. & Koay, E. S. Phosphorylation of Ser78 of Hsp27 correlated with HER-2/neu status and lymph node positivity in breast cancer. *Mol Cancer* **6**, 52 (2007).

AUTHOR CONTRIBUTIONS

L.W.: Conceptualization, Methodology, Writing- Original draft preparation, Investigation, Validation. S.W.: Methodology, Visualization. H.H.: Software, Data curation. K.A.: Data curation, Validation. R.X.: Methodology, Validation. L.Z.: Software, Visualization. X.Z.: Conceptualization, Writing- Original draft preparation, Supervision, Writing-Reviewing and Editing.

FUNDING

This work was supported by Hunan Provincial Natural Science Foundation of China (No. 2019JJ40442), National Natural Science Foundation of China (Grant no. 81972195), Hunan Provincial Key Area R&D Program (Grant no. 2019SK2253), Scientific Research Program of Hunan Provincial Health Commission (Grant no. 20201047) and Clinical Medical Technology Innovation Guide Project of Hunan Province (grant number S2020SFYLJS0311).

COMPETING INTERESTS

The authors declare no competing interests.

ETHICS APPROVAL AND CONSENT TO PARTICIPATE

Nude mice (male, 7–8 weeks old) were provided by Hunan SJA Laboratory Animal Co., Ltd, animal experiments were performed in accordance with the guidelines of the Committee on the Ethics of Animal Experiments of Central South University.

ADDITIONAL INFORMATION

Supplementary information The online version contains supplementary material available at https://doi.org/10.1038/s41374-022-00826-3.

Correspondence and requests for materials should be addressed to Xuan Zhu.

Reprints and permission information is available at http://www.nature.com/reprints

Publisher's note Springer Nature remains neutral with regard to jurisdictional claims in published maps and institutional affiliations.